arXiv:1203.6182v3 [cond-mat.other] 16 Aug 2012

Thermally- and mechanically-driven quantum turbulence in helium II

A. W. Baggaley,[1] L. K. Sherwin,[1] C. F. Barenghi,[1] and Y. A. Sergeev[2]

[1] *Joint Quantum Centre Durham-Newcastle, School of Mathematics and Statistics, University of Newcastle, Newcastle upon Tyne, NE1 7RU, UK*

[2] *Joint Quantum Centre Durham-Newcastle, School of Mechanical and Systems Engineering, Newcastle University, Newcastle upon Tyne, NE1 7RU, UK*

In most experiments with superfluid helium turbulence is generated thermally (by applying a heat flux, as in thermal counterflow) or mechanically (by stirring the liquid). By modelling the superfluid vortex lines as reconnecting space curves with fixed circulation, and the driving normal fluid as a uniform flow (for thermal counterflow) and a synthetic turbulent flow (for mechanically-driven turbulence), we determine the difference between thermally-driven and mechanically-driven quantum turbulence. We find that in mechanically-driven turbulence the energy is concentrated at the large scales, the spectrum obeys Kolmogorov scaling, vortex lines have large curvature, and the presence of coherent vortex structures induces vortex reconnections at small angles. On the contrary, in thermally-driven turbulence the energy is concentrated at the mesoscales, the curvature is smaller, the vorticity field is featureless and reconnections occur at larger angles. Our results suggest a method to experimentally detect the presence of superfluid vortex bundles.

I. INTRODUCTION

Recent work [1, 2] has highlighted similarities between the turbulence of superfluid helium II (quantum turbulence) and the turbulence of ordinary (classical) fluids. In particular, experimental [3, 4] and theoretical [5–11] studies have established that the distribution of the superfluid kinetic energy over the length scales (energy spectrum) obeys the same $k^{-5/3}$ Kolmogorov scaling of ordinary turbulence [12] where k is the wavenumber. The similarity is remarkable because helium II is unlike an ordinary fluid: firstly, it has a two-fluid nature, consisting of a viscous normal fluid component and an inviscid superfluid component coupled by a mutual friction [13]; secondly, superfluid vorticity is not a continuous field (like in an ordinary fluid) but is restricted to discrete vortex filaments around which the circulation is fixed to the ratio of Planck's constant and the mass of one helium atom.

In most experiments turbulence in helium II is excited mechanically (by stirring the helium with grids or propellers [3, 4, 14] or forcing it along pipes [15]), or thermally (by the application of a heat flux [16, 17]). The simplest, most studied form of thermal stirring (to which hereafter we restrict our work) is called thermal counterflow. The name arises because the normal fluid and the superfluid move in opposite directions, so that their velocity difference is proportional to the applied heat flux and the net mass flux is zero. Other forms of heat transfer (e.g. pure superflow) and other techniques to generate turbulence (e.g. ultrasound [18], ion injection and spin-downs [19]) are either less studied, or refer to the low temperature limit (below 1 K), or have a special character (rotating turbulence, turbulent fronts, the Kibble-Zurek mechanism, etc.). thus they are not our interest here, and nor are the special methods used to model them; for these aspects we refer the reader to a recent review [20].

The aim of this work is to clarify the difference between thermally-excited counterflow turbulence and mechanically-excited turbulence in helium II. For simplicity, we are concerned only with statistical steady state turbulence away from boundaries (thus ignoring the important problems of turbulence decay and flow profiles), and at the relatively high temperatures, where mutual friction plays a role.

After setting up the necessary numerical models (section II) we compute for the first time the energy spectrum of counterflow turbulence, compare it to the spectrum of mechanically-driven turbulence, and test the idea which has been proposed in the literature that "counterflow turbulence has only one length scale", meaning the average intervortex distance (section III). We also find that thermally- and mechanically-induced turbulence differ with respect to curvature (section IV), the presence of coherent structures (section V) and vortex reconnection statistics. The last result suggests a method to detect experimentally the existence of superfluid vortex bundles (section VI). Section VII summarises the conclusions.

II. NUMERICAL METHOD

Following Schwarz [21], we model quantum vortex filaments as space curves $\mathbf{s}(\xi, t)$ which move according to

$$\frac{d\mathbf{s}}{dt} = \mathbf{v}_s^{tot} + \alpha \mathbf{s}' \times (\mathbf{v}_n^{ext} - \mathbf{v}_s^{tot}) - \alpha' \mathbf{s}' \times (\mathbf{s}' \times (\mathbf{v}_n^{ext} - \mathbf{v}_s^{tot})), \tag{1}$$

where t is time, α and α' are temperature dependent friction coefficients [22], $\mathbf{s}' = d\mathbf{s}/d\xi$ is the unit tangent vector at the point $\mathbf{s}$, ξ is arc length, and $\mathbf{v}_n^{ext}$ and $\mathbf{v}_s^{ext}$ are externally applied normal fluid and superfluid velocities. The self-induced velocity of the vortex filament at the point $\mathbf{s}$ is given by the Biot-Savart law [23]

$$\mathbf{v}_s^i = -\frac{\kappa}{4\pi} \oint_{\mathcal{L}} \frac{(\mathbf{s} - \mathbf{r})}{|\mathbf{s} - \mathbf{r}|^3} \times \mathbf{dr}, \tag{2}$$

where $\kappa = 9.97 \times 10^{-4}$ cm^2/s is the quantum of circulation and the line integral extends over the entire vortex configuration $\mathcal{L}$. The total superfluid velocity is thus $\mathbf{v}_s^{tot} = \mathbf{v}_s^i + \mathbf{v}_s^{ext}$.

In the case of thermal counterflow (which hereafter we simply refer to as thermally-driven, to contrast it to mechanically-driven turbulence), $\mathbf{v}_n^{ext}$ and $\mathbf{v}_s^{ext}$ arise from the imposed heat flux $\dot{Q}$, where $v_{ns} = |\mathbf{v}_n^{ext} - \mathbf{v}_s^{ext}| = \dot{Q}/(\rho_s S T)$ is the counterflow velocity, $v_n^{ext} = \dot{Q}/(\rho S T)$, $v_s^{ext} = -\rho_n v_n^{ext}/\rho_s$, S is the specific entropy, T is the temperature, ρ_s and ρ_n are the superfluid and normal fluid densities, and $\rho = \rho_s + \rho_n$. We make the usual [21, 24] simplifying assumption of uniform velocity profiles $\mathbf{v}_n^{ext}$ and $\mathbf{v}_s^{ext}$ away from boundaries, neglecting the possibility that at sufficiently large $\dot{Q}$ the normal fluid becomes turbulent [25, 26]. It is also convenient to perform the calculation in the frame of reference of the imposed superflow, setting $\mathbf{v}_s^{ext} = 0$.

In the case of mechanically-induced turbulence, since we ignore boundaries and flow profiles, we set $\mathbf{v}_s^{ext} = \mathbf{0}$ in Eq. (1) and replace $\mathbf{v}_n^{ext}$ with the following synthetic turbulent flow [27]:

$$\mathbf{v}_n^{ext}(\mathbf{s},\, t) = \sum_{m=1}^{m=M} (\mathbf{A}_m \times \mathbf{k}_m \cos\phi_m + \mathbf{B}_m \times \mathbf{k}_m \sin\phi_m), \tag{3}$$

where $\phi_m = \mathbf{k}_m \cdot \mathbf{s} + \omega_m t$, $\mathbf{k}_m$ and $\omega_m = \sqrt{k_m^3 E(k_m)}$ are wave vectors and angular frequencies. This $\mathbf{v}_n^{ext}$ is solenoidal, time-dependent, and, with a suitable choice of $\mathbf{A}_m$ and $\mathbf{B}_m$ (adapted to the periodic box [28]), its energy spectrum has Kolmogorov form $E(k_m) \sim k_m^{-5/3}$ in the range from k_1 (corresponding to the integral scale) to k_M (corresponding to the dissipation scale). Synthetic turbulence is widely used to study transport properties, and compares very well with direct numerical simulations and experiments (for example it satisfies observed two-points turbulence statistics).

Our calculations are performed in a periodic cube of size $D = 0.1$ cm. The numerical techniques to discretize the vortex filaments into a variable number of points $\mathbf{s}_j$ $(j = 1, \cdots N)$ held at minimum separation $\Delta\xi/2$, compute the time evolution, de-singularize the Biot-Savart integrals, evaluate $\mathbf{v}_s^i$ using a tree-method (with critical opening angle 0.4), and algorithmically perform vortex reconnections when vortex lines come sufficiently close to each other, are all described in our previous papers [9, 29–31].

It must be stressed that our models have a limitation: the normal fluid is prescribed rather than computed self-consistently. The inclusion of the back-reaction of the superfluid vortices onto the normal fluid would require the numerical solution of the Navier-Stokes equation for the normal fluid (suitably modified by the inclusion of a mutual friction term), alongside the time evolution of the superfluid vortices. However, a dynamically self-consistent model would be very complex and computationally expensive, and one could not easily explore parameter space and the effects of changing numerical resolution and initial conditions. This approach was attempted for a single vortex ring [32]. In the case of turbulence, this approach has so far been limited to the initial growth of a cloud of vortex lines [33].

III. ENERGY SPECTRUM

We choose temperature $T = 1.9$ K (at which $\alpha = 0.206$ and $\alpha' = 0.0083$) which is typical of experiments and allows direct comparison with previous work, and numerical resolution $\Delta\xi = 0.0016$ cm. First we calculate thermally-induced turbulent vortex tangles at increasing values of v_{ns}. We find that, after an initial transient, the vortex line density L (vortex length per unit volume) saturates to a statistically steady state (see Fig. 1) of density $L = \gamma^2 v_{ns}^2$ which is independent of the details of the initial condition (various vortex loops configurations were tried). Fig. 2 (top) shows a snapshot of such vortex tangle.

Our vortex line densities agree with previous work; for example, taking $T = 1.9$ K we obtain $\gamma \approx 137$ s/cm^2 which compares well to $\gamma \approx 140$ and 133 obtained in the numerical simulations of Adachi *et al.* [24] and in the experiments of Childers and Tough [34] respectively.

To analyze our results we Fourier-transform the superfluid velocity and compute the energy spectrum E_k. If the turbulence is isotropic, E_k is defined by

$$E = \frac{1}{V}\int_V \frac{1}{2}\mathbf{v}_s^2 dV = \int_0^\infty E_k dk, \tag{4}$$

where V is volume, $k = |\mathbf{k}|$, and $\mathbf{k}$ is the three-dimensional wavenumber. However, it is well known [21, 24] that counterflow turbulence is flattened on the $(y,\, z)$ plane perpendicular to the direction (x) of the heat flux. For example, if L_x, L_y and L_z are the vortex lengths (per unit volume) projected in the x, y and z-direction, at $v_{ns} = 1.25$ cm/s we have $L_x/L = 0.34 < L_y/L = 0.55 = L_z/L$. It is therefore better to distinguish between parallel and perpendicular superfluid energy spectra, $E_\parallel$ and $E_\perp$, calculated replacing $\mathbf{v}_s^2 = v_{sx}^2 + v_{sy}^2 + v_{sz}^2$ in Eq. (4) with $3v_{sx}^2$ and $(3/2)(v_{sy}^2 + v_{sz}^2)$ respectively. Fig. 3 (top) shows $E_\perp$ for various v_{ns} plotted in the range $k_D = 2\pi/D \le k_\perp \le k_{\Delta\xi} = 2\pi/\Delta\xi$ (where $k_\perp$ is the perpendicular wavevector); the vertical lines mark the wavenumbers $k_\ell = 2\pi/\ell$ corresponding to the average intervortex spacing, $\ell \approx L^{-1/2}$. It is apparent that the perpendicular energy spectrum $E_\perp$ has a broad peak in the mesoscales at intermediate wavenumbers $k_D < k < k_\ell$. At larger k the spectrum follows the typical k^{-1} scaling of smooth isolated vortex lines as expected. The parallel spectrum $E_\parallel$ vs $k_\parallel$ (where $k_\parallel$ is the parallel wavevector) exhibits similar features, see Fig. 3 (bottom). Plotting $E_\perp$ and $E_\parallel$ vs k rather than $k_\perp$ and $k_\parallel$ yields similar results. We note that the counterflow energy spectrum, which we measure, is qualitatevely similar to the spectrum shown by Nemirovskii, Tsubota and Araki [35] in their Fig.2.

Proceeding in analogy to what we did for counterflow turbulence, we start from an arbitrary seeding initial condition, drive the vortex tangle with the synthetic turbulent flow of Eq. (3), and let L grow and saturate to a statistical steady

state of turbulence which does not depend on the initial condition (the time behaviour of L is similar to Fig. 1). A snapshot of this mechanically-driven tangle is shown in Fig. 2 (bottom). We then compute the superfluid energy spectrum. In agreement with previous experimental [3, 4] and theoretical [9, 11] work, we find that the energy is concentrated at the largest scales, $k \approx k_D$, and that $E_k \sim k^{-5/3}$ for large k (see Fig. 4).

We conclude that there is a remarkable spectral difference between thermally-driven turbulence and mechanically-driven turbulence. Whereas in the former the turbulent kinetic energy is concentrated at intermediate length scales, in the latter most of the energy is at the largest scales, as in classical ordinary turbulence.

An argument is often made in the literature that counterflow turbulence has only one characteristic length scale, the intervortex distance ℓ: it is apparent from Fig. 3 that E_k does not have a sharp peak at $k \approx k_\ell = 2\pi/\ell$ (indicated by the vertical lines), but rather a broad maximum at smaller wavenumbers in the mesoscale region $k_D < k \leq k_\ell$. The traditional argument, although quantitatively wrong, is thus qualitatively correct.

IV. CURVATURE

If we look carefully at the vortex tangles shown in Fig. 2, we notice that the thermally-driven tangle (top) contains relatively more closed loops, and the mechanically-driven tangle (bottom) contains relatively more long vortices which extend throughout the periodic computational domain. We sample the curvature $C = |\mathbf{s}''|$ along each vortex loop and construct the probability density function (PDF) of the mean curvature $\bar{C}$ of each distinct loop. Fig. 5 shows the result. We notice that mechanically-driven turbulence contains smaller curvatures (that is, larger radii of curvature $R = 1/C$) than thermally-driven turbulence; indeed, for the latter PDF($\bar{C}$) has a maximum at $\bar{C} \approx 250$ in correspondence of the maximum of the energy spectrum shown in Fig. 3.

As an additional numerical experiment, we compute the energy spectra of configurations of circular vortex rings placed randomly in the periodic box of size D as a function of the rings' radius R. We find that if $R \geq D$ (in which case rings are "folded" into broken arches by the periodic boundary conditions) most of the energy is concentrated at the largest length scales, whereas if $R < D$ the energy spectrum peaks at intermediate scales, in analogy with the counterflow spectrum.

V. COHERENT STRUCTURES

We also notice another difference between the two forms of turbulence. If we convolve the vortex filaments with a Gaussian kernel and define a smoothed vorticity field $\boldsymbol{\omega}_s$ (the details of the procedure are described in Ref. [10]), it becomes apparent - see Fig. 6 - that the thermally-induced tangle (sustained by the uniform $\mathbf{v}_n^{ext}$) is essentially featureless, whereas the mechanically-induced tangle (sustained by the turbulent $\mathbf{v}_n^{ext}$) contains "vortical worms", or regions of concentrated vorticity - see Fig. 7. This result is consistent with the observation of "worms" in two other related turbulent flows: ordinary viscous turbulence [12] and pure superfluid turbulence at $T = 0$ without the normal fluid [10]; both flows satisfy the Kolmogorov $k^{-5/3}$ scaling.

It is known from previous work that if intense regions of normal fluid vorticity are imposed, such as Gaussian vortex tubes [36], ABC flows [37] or worms [38, 39], these structures will induce (via the friction force) similar structures in the superfluid vortex lines. Our synthetic turbulent flow $\mathbf{v}_n^{ext}$, although not completely featureless on its own, contains only weak vortex structures, much smaller [40] than the vortical worms arising from direct numerical simulations of the Navier-Stokes equation. Therefore the observation of superfluid vortex bundles driven by the synthetic turbulent flow $\mathbf{v}_n^{ext}$ of Eq. (3) must be an underestimate of the strength of these bundles. If we solved the Navier-Stokes equation for the normal fluid (rather than imposing $\mathbf{v}_n^{ext}$), the normal fluid's worms would probably "imprint" vortex bundles in the superfluid, besides the bundles which arise naturally in the superfluid as a consequence of Euler dynamics [10].

A tentative explanation of the observation that the vortex configuration is rather homogeneous for thermally-driven turbulence and inhomogeneous for mechanically-driven turbulence is that in the former (assuming, as we do, a uniform normal flow) the growth rate of the Donnelly-Glaberson (DG) instability (which transforms normal fluid's energy into superfluid vortex length) is the same everywhere, whereas in the latter it changes with time and space.

The DG mechanism is the following [41]. If it is large enough, the component V of the normal fluid velocity along a vortex lines can destabilise a (helical) Kelvin wave of given wavenumber k. In this case, the Kelvin wave grows with amplitude $\mathcal{A}(t) = \mathcal{A}(0)e^{\sigma t}$, where $A(0)$ is the initial amplitude of the helix and

$$\sigma(k) = \alpha(kV - \nu' k^2) \tag{5}$$

is the growth rate, $\nu' = \kappa\mathcal{L}_1/(4\pi) \approx \kappa$, and $\mathcal{L}_1 = \ln[1/(ka_0)]$. The growth of the Kelvin wave, however, may be interrupted by a vortex reconnection which "breaks" the vortex line. It is known that vortex reconnections play an

essential role in the turbulence [21, 42, 43]. Therefore, it is prudent to assess the effect of reconnections on the DG instability.

Consider mechanically-driven turbulence in a statisticaly steady state at $T = 1.9$ K ($\alpha = 0.206$) driven by the rms normal fluid velocity $V \approx 0.93$ cm/s, with average vortex length $\Lambda \approx 11.5$ cm, vortex line density $L \approx 1.15 \times 10^4$ cm^{-2}, and intervortex spacing $\ell \approx 9.3 \times 10^{-3}$ cm, and thermally-driven turbulence at the same temperature with $V = 0.75$ cm/s, $\Lambda \approx 11.88$ cm, $L \approx 1.19 \times 10^4$ cm^{-2}, and $\ell \approx 9.2 \times 10^{-3}$. The average number ζ of vortex reconnections per unit time is monitored during the numerical calculations; we obtain $\zeta \approx 4370$ and 7386 s^{-1} for mechanically and thermally driven turbulence, respectively (in reasonable agreement with the estimate $\zeta \approx (2/3)\kappa L^{5/2} \approx 9500$ s^{-1}, for a homogeneous isotropic tangle, of Barenghi & Samuels [44]).

The mode which undergoes the most rapid DG instability has wavenumber $k_{\max} = V/(2\nu')$ and growth rate $\sigma_{\max} = \alpha V^2/(4\nu')$, corresponding to the length scale $d_{\max} = 2\pi/k_{\max}$. In both mechanically-driven and thermally-driven cases this length scale ($d_{\max} = 0.015$ and 0.017 cm respectively) is larger than than the average distance between vortices ℓ, and so not suitable for our analysis. We therefore perform an analysis for Kelvin waves with a wavelength and a wavenumber equal to ℓ and $k_\ell = 2\pi/\ell$, respectively; we assume that such waves are the lowest frequency waves in our system. The growth rate of such a waves is $\sigma_{DG} = \sigma(k_\ell)$, where $\sigma(k)$ is defined in Eq. (5).

The reconnection rate ζ computed during the simulations is a statistical property of the vortex tangle as a whole. However we can compute a reconnection frequency for a wavenumber and wave amplitude by scaling the total reconnection rate by the fraction of the total vortex length that a given wavelength takes. In such a manner we define

$$\sigma_r(\mathcal{A}) = \frac{\zeta}{\Lambda} \int_0^\ell \left[1 + (\mathcal{A}k_\ell)^2 \cos^2(k_\ell x)\right]^{-1/2} dx. \tag{6}$$

Fig. 8 shows the ratio σ_{DG}/σ_r vs wave amplitude $\mathcal{A}$ for the two simulations described above. We note a large contrast in the behaviour of the ratio of these two timescales when comparing the mechanically and thermally driven cases. For the latter one would estimate that the amplitude of perturbations along the vortices can grow to approximately the intervortex spacing before reconnections dominate the behaviour of the tangle. However, in the mechanically driven case $\sigma_{DG} \approx \sigma_r$ for $\mathcal{A} \approx D/3$ so that the large amplitude perturbations are able to grow, before reconnections randomise the tangle and introduce topological changes. Therefore the difference in the balance between these two competing timescales is likely to be partially responsible for the differences in the nature of the two turbulent systems.

VI. VORTEX RECONNECTIONS

The existence of superfluid vortex bundles [36–39], their dynamics [45] and their particular significance at very low temperatures [46, 47] have been discussed in the literature, but so far there is no clear experimental evidence for them. It has been argued that the presence of bundles of locally almost parallel vortices (which we have demonstrated in the previous section for mechanically-induced turbulence) leads to a suppression of vortex reconnections [46, 47].

In the vortex filament model, vortex reconnections are performed algorithmically; the details are described in Ref. [31]. Within the approximation, intrinsic to the model, it is instructive to study the distribution of the angles θ between reconnecting vortex lines at the level of discretization which we use (which is necessarily much larger than a_0). The normalised distribution of values of θ, PDF(θ), is shown in Fig. 9: the solid black line with black circles refers to mechanically-driven turbulence, and the solid red line with red squares to thermally driven turbulence. It is apparent that in thermally-induced turbulence the majority of vortex reconnections take place between vortex filaments which are nearly anti-parallel ($\theta \approx \pi$), whereas in mechanically-driven turbulence most reconnections are between vortices which are nearly parallel ($\theta < \pi/2$). Our results confirm that indeed the presence of organised bundles of vortices changes the typical geometry of reconnections.

To check the temperature dependence of the results we repeat our calculations at higher temperature, $T = 2.1$ K. At this temperature the friction coefficients are larger ($\alpha = 1.21$ and $\alpha' = -0.3883$), therefore a more intense vortex tangle is generated at the same value of the drive; moreover, short Kelvin waves are damped out more quickly. We check that at the higher temperature $T = 2.1$ K the same differences between thermally-driven and mechanically-driven turbulence are present, which we have described in the previous sections for $T = 1.9$ K in terms of energy spectrum, curvature and coherence structures. Fig. 9 shows that, qualitatively, the distribution of reconnecting angles is also temperature independent (the black solid line, which refers to mechanically-driven turbulence peaks at small θ, the solid red line which refers to thermally-driven turbulence peaks at large θ).

This result could be exploited to look for experimental evidence of superfluid vortex bundles in the following way. Using solid hydrogen tracer particles to visualise the vortex lines, Paoletti, Fisher and Lathrop *et al.* [48] determined that the the minimum distance $\delta(t)$ between vortex lines before and after a reconnection scales as

$$\delta(t) = A(\kappa|t - t_0|)^{1/2}(1 + c|t - t_0|), \tag{7}$$

where t_0 is the time at which the reconnection takes place, with fitting coefficients $A \approx 1.2$ and $c \approx 0$. We proceed in this way, monitoring vortex reconnections in our numerical calculations. Fig. 10 shows the probability density functions of our fitting parameters A and c obtained for 1107 reconnections in thermally-driven turbulence (average values $\langle A \rangle = 2.6$ and $\langle c \rangle = 1.6$) and 879 reconnections in mechanically-driven turbulence (average values $\langle A \rangle = 1.8$ and $\langle c \rangle = 0.7\,\mathrm{s}^{-1}$). Our fitting coefficients thus agree fairly well with the experimental findings of Ref. [48] and with the numerical results of Tsubota and Adachi [49] ($A \approx 3$ and $c \approx 0\,\mathrm{s}^{-1}$).

Fig. 10 shows that the distribution of values of A is different for thermally-driven and mechanically-driven turbulence. The effect must arise from the different distributions of curvature and reconnecting angles θ for vortex bundles, which are present only in mechanically-driven turbulence. This is confirmed by Fig. 11, which displays scatter plots of the fitting parameters A (top) and c (middle). Fig. 11 also shows the angular dependence of the mean curvature $\bar{\mathcal{C}}_r$ (bottom) of the reconnecting vortex segments.

It is clear that the curvature of the filaments after a reconnection is dependent on the angle of the reconnection. From inspection of the local induction approximation [23] we would expect larger velocities (and thus A) with increased curvature, as we observe in the numerical simulations. These result suggests a possible experimental strategy to establish the existence of vortex bundles based on the careful analysis of the reconnection fitting parameter A.

VII. CONCLUSIONS

In conclusion, we have addressed for the first time the question of the energy spectrum of thermally-induced counterflow turbulence, and found that it is unlike the spectrum of turbulence generated mechanically. More in general, we have found that the two forms of quantum turbulence which can be generated in superfluid helium are quite different. Counterflow turbulence, driven thermally by a constant normal fluid velocity, is uniform in physical space and the energy spectrum is concentrated at intermediate wavenumbers k. On the contrary, quantum turbulence driven mechanically by a turbulent normal fluid contains regions of concentrated coherent vorticity and vortex lines with larger radii of curvature; the energy is concentrated at the largest scales, exhibiting the same $k^{-5/3}$ scaling of ordinary turbulence which suggests the presence of an energy cascade. Our results prove that counterflow turbulence, a form of disordered heat transfer unique to liquid helium, lacks the multitude of interacting length scales which is perhaps the main property of ordinary turbulence. Vortex reconnections are affected by the presence of bundles of almost parallel vortices, suggesting an experimental technique to detect these bundles based on monitoring the vortex separation after reconnections.

ACKNOWLEDGMENTS

We thank the Leverhulme Trust and the EPSRC for financial support.

[1] L. Skrbek and K. R. Sreenivasan, Phys. Fluids **24**, 011301 (2012).
[2] W. F. Vinen and J. J. Niemela, J. Low Temp. Phys. **128**, 167 (2002).
[3] J. Maurer and P. Tabeling, Europhys. Lett. **43**, 29 (1998).
[4] J. Salort *et al.*, Phys. Fluids **22**, 125102 (2010).
[5] C. Nore, M. Abid, and M. E. Brachet, Phys. Rev. Lett. **78**, 3896 (1997).
[6] T. Araki, M. Tsubota, and S. K. Nemirovskii, Phys. Rev. Lett. **89**, 145301 (2002).
[7] M. Kobayashi and M. Tsubota, Phys. Rev. Lett. **94**, 065302 (2005).
[8] N. Sasa *et al.* Phys. Rev. B **84**, 054525 (2011).
[9] A. W. Baggaley and C. F. Barenghi, Phys. Rev. B **84**, 020504 (2011).
[10] A. W. Baggaley, C. F. Barenghi, A. Shukurov, and Y. A. Sergeev, Europhys. Lett. **98**, 26002 (2012).
[11] V. S. L'vov, S. V. Nazarenko, and L. Skrbek, J. Low Temp. Phys. **145**, 125 (2006).
[12] U. Frisch, *Turbulence. The legacy of A.N. Kolmogorov* (Cambridge University Press, Cambridge, England, 1995).
[13] R. J. Donnelly, *Quantized Vortices in Helium II* (Cambridge University Press, Cambridge, England, 1991).
[14] M. R. Smith, R. J. Donnelly, N. Goldenfeld, and W. F. Vinen, Phys. Rev. Lett. **71**, 2583 (1993).
[15] P. L. Walstrom, J. G. Weisend, J. R. Maddocks, and S. W. Van Sciver, Cryogenics **28**, 101 (1988).
[16] W. F. Vinen, Proc. Roy. Soc. A**240**, 114 (1957); W. F. Vinen, Proc. Roy. Soc. A**240**, 128 (1957); W. F. Vinen, Proc. Roy. Soc. A**242**, 494 (1957); W. F. Vinen, Proc. Roy. Soc. A**243**, 400 (1957).
[17] J. Tough, *Progress in Low Temp. Physics* (North-Holland, Amsterdam, 1982). Vol. VIII, Chap. 3, p. 133.
[18] K. W. Schwarz and C. W. Smith, Phys. Lett. A **82** 251 (1981).
[19] P. M. Walmsley and A. I. Golov, Phys. Rev. Lett. **100**, 245301 (2008).
[20] M. Tsubota and W.P. Halperin, eds, *Progress in low temperature physics: quantum turbulence*, vol. XVI, Elsevier, Amsterdam (2009).
[21] K. W. Schwarz, Phys. Rev. B **38**, 2398 (1988).
[22] R. J. Donnelly and C. F. Barenghi, J. Phys. Chem. Ref. Data **27**, 1217 (1998).
[23] P. G. Saffman, *Vortex Dynamics* (Cambridge University Press, Cambridge, England, 1992).
[24] H. Adachi, S. Fujiyama, and M. Tsubota, Phys. Rev. B **81**, 104511 (2010).
[25] D. J. Melotte and C. F. Barenghi, Phys. Rev. Lett. **80**, 4181 (1998).
[26] W. Guo et al., Phys. Rev. Lett. **105**, 045301 (2010).
[27] D. R. Osborne, J. C. Vassilicos, K. Sung, and J. D. Haigh, Phys. Rev. E **74**, 036309 (2006).
[28] S. L. Wilkin, C. F. Barenghi, and A. Shukurov, Phys. Rev. Lett. **99**, 134501 (2007).
[29] A. W. Baggaley and C. F. Barenghi, Phys. Rev. B **83**, 134509 (2011).
[30] A. W. Baggaley and C. F. Barenghi, J. Low Temp. Physics **166**, 3 (2012).
[31] A. W. Baggaley, J. Low Temp. Physics **168**, 18 (2012).
[32] D. Kivotides, C.F. Barenghi and D.C. Samuels, Science, **290**, 777 (2000).
[33] D. Kivotides, J. Fluid Mechanics, **668**, 58 (2011).
[34] R. K. Childers and J. T. Tough, Phys. Rev. B **13**, 1040 (1976).
[35] S.K. Nemirovskii, M. Tsubota, and T. Araki, J. Low Temp. Phys. **126**, 1535 (2002)
[36] D. C. Samuels, Phys. Rev. B **47**, 1107 (1993).
[37] C. F. Barenghi, G. H. Bauer, D. C. Samuels, and R. J. Donnelly, Phys. Fluids **9**, 2631 (1997).
[38] D. Kivotides, Phys. Rev. Lett. **96**, 175301 (2006).
[39] K. Morris, J. Koplik, and D. W. Rouson, Phys. Rev. Lett. **101**, 015301 (2008).
[40] J. C. K. Fung, J. C. R. Hunt, N. A. Malik, and R. J. Perkins, J. Fluid Mech. **236**, 281 (1992).
[41] M. Tsubota, C. F. Barenghi, T. Araki, and A. Mitani, Phys. Rev. B **69**, 134515 (2004).
[42] R.P. Feynman, "Application of quantum mechanics to liquid helium", in *Progress in Low Temperature Physics*, edited by C. J. Gorter (North-Holland, Amsterdam, 1955), Vol 1.
[43] S.K. Nemirovskii, Phys. Rev. B **77**, 214509 (2008).
[44] C.F. Barenghi and D.C. Samuels, J. Low Temp. Phys. **136**, 281 (2004).
[45] S. Z. Alamri, A. J. Youd, and C.F. Barenghi Phys. Rev. Lett. **101**, 215302 (2008).
[46] V. S. L'vov, S. V. Nazarenko, and O. Rudenko, Phys. Rev. B **76**, 024520 (2007).
[47] E. Kozik and B. Svistunov, Phys. Rev. B **77**, 060502 (2008).
[48] M. S. Paoletti, M.E. Fisher, and D.P. Lathrop, Physica D **239**, 1367 (2010).
[49] M. Tsubota and H. Adachi, J. Low Temp. Physics **162**, 367 (2011).

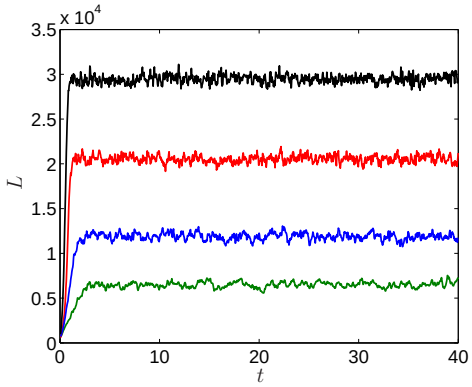

FIG. 1. (Color online) Thermally-induced turbulence. The evolution of the vortex line density L (cm^{-2}) vs time t (s) at counterflow velocities (from top to bottom) $v_{ns} = 1.25$ cm/s (black), 1.0 cm/s (red), 0.75 cm/s (blue), and 0.55 cm/s (green).

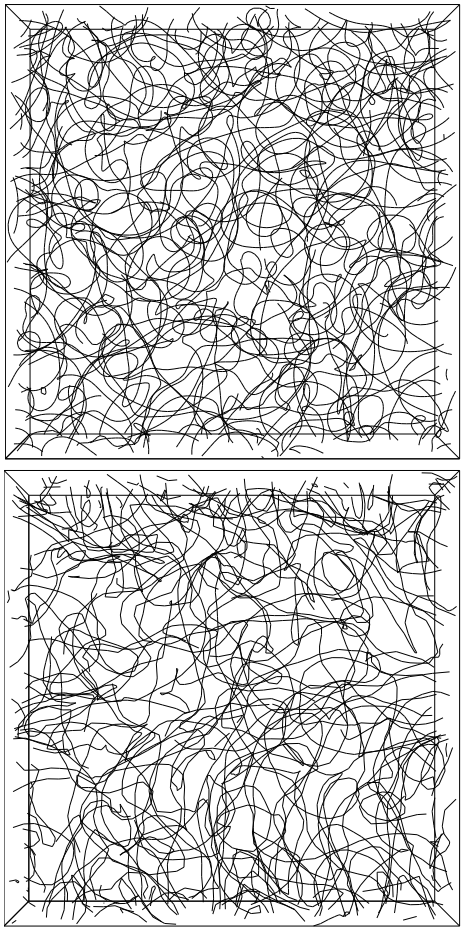

FIG. 2. Snapshots of vortex tangles (y, z projections). Top: thermally-driven by counterflow ($v_{ns} = 0.75$ cm/s, $L \approx 12000$ cm^{-2}); bottom: mechanically-driven ($Re = 208$, $L \approx 12000$ cm^{-2})

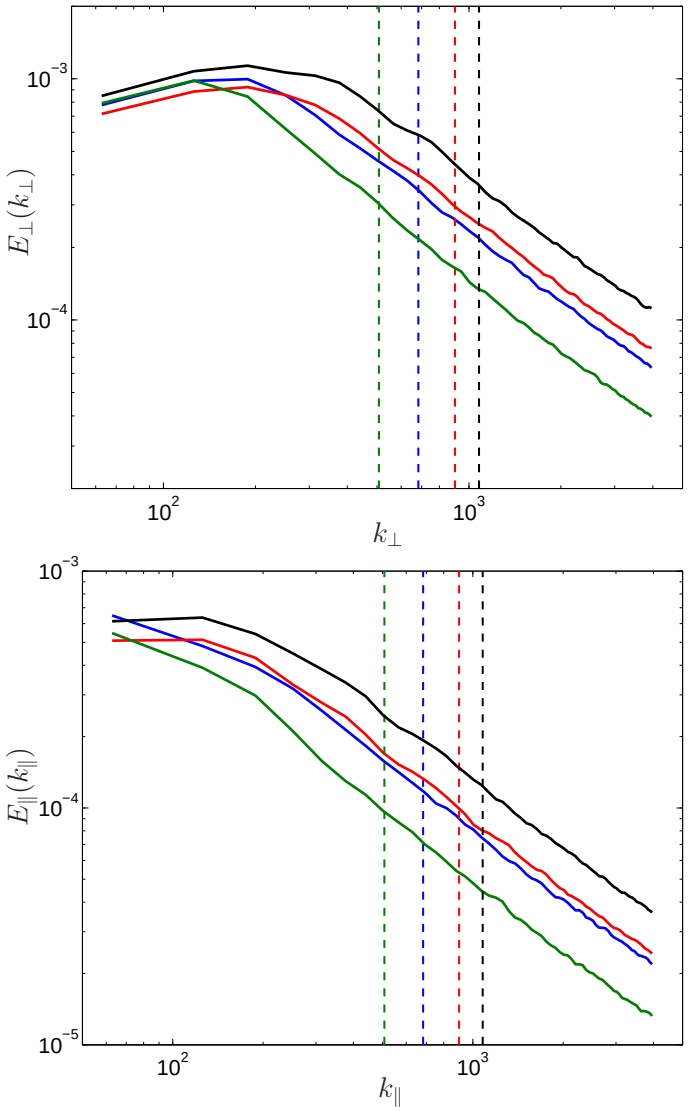

FIG. 3. (Color online) Counterflow turbulence. Top: the perpendicular energy spectrum $E_\perp(k_\perp)$ (arbitrary units) vs wavenumber $k_\perp$ (cm^{-1}). Bottom: the parallel energy spectrum $E_\parallel(k_\parallel)$ (arbitrary units) vs wavenumber $k_\parallel$ (cm^{-1}). The vertical lines mark k_ℓ at increasing v_{ns} from right to left.

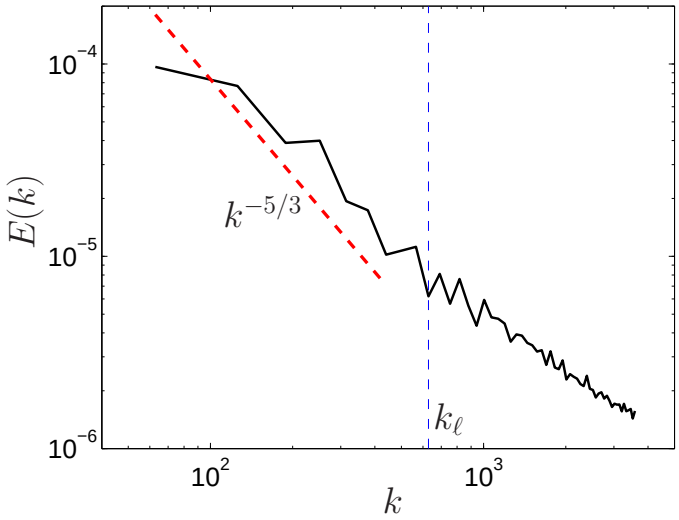

FIG. 4. (Color online) Mechanically-induced turbulence. Energy spectrum E_k (arbitrary units) vs wavenumber k (cm^{-1}) of vortex tangle driven by the synthetic turbulent flow of Eq. (3) with $M = 188$ modes. The vertical dashed blue line marks k_ℓ. The dashed red line shows the $k^{-5/3}$ Kolmogorov scaling. The effective Reynolds number of the normal fluid is $Re = (k_M/k_1)^{4/3} = 208$, defined by the condition that the dissipation time equals the eddy turnover time at k_M.

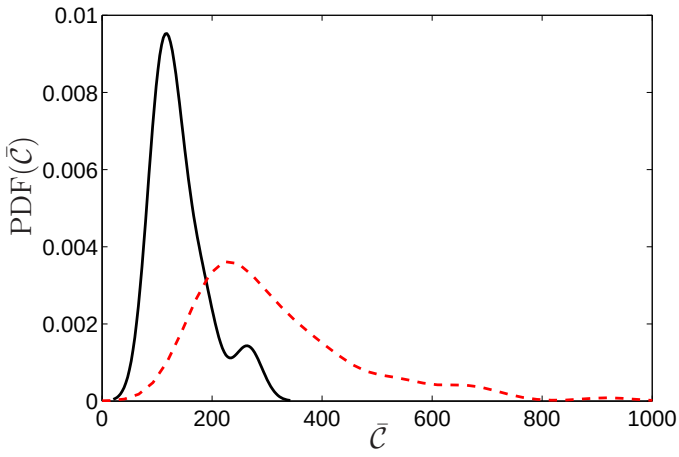

FIG. 5. Probability density function (PDF) of the mean curvature per vortex loop $\bar{C}$. Solid black line: mechanically-driven turbulence; dashed red line: thermally-driven turbulence. Notice the larger curvatures present in thermally-driven turbulence.

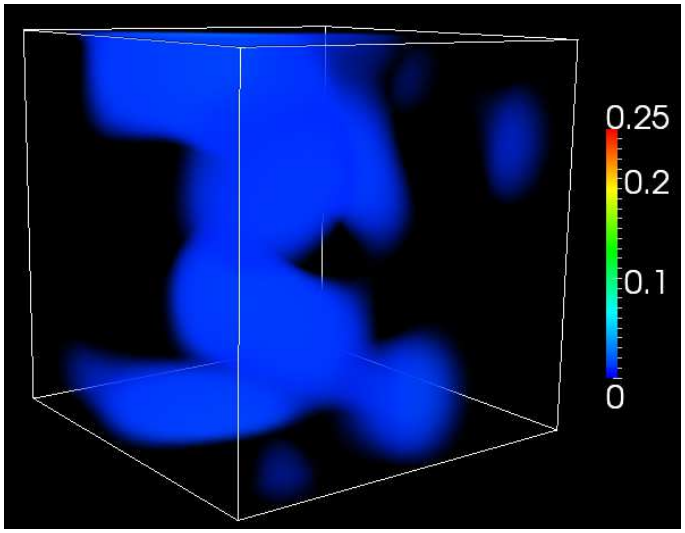

FIG. 6. (Color online) Smoothed vorticity $\boldsymbol{\omega}$ sustained by a constant $\mathbf{v}_n^{ext}$ (thermally-driven turbulence).

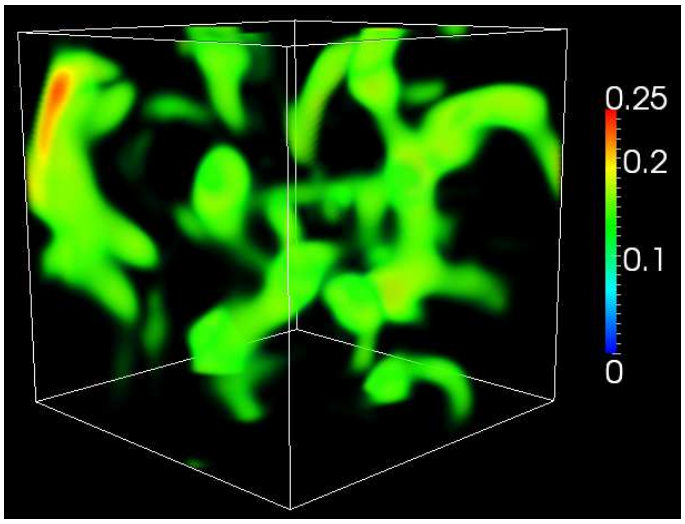

FIG. 7. (Color online) Smoothed vorticity $\boldsymbol{\omega}$ sustained by a turbulent $\mathbf{v}_n^{ext}$ (mechanically-driven turbulence). Notice the intense vortical regions compared to Fig. 6 which is plotted on the same scale.

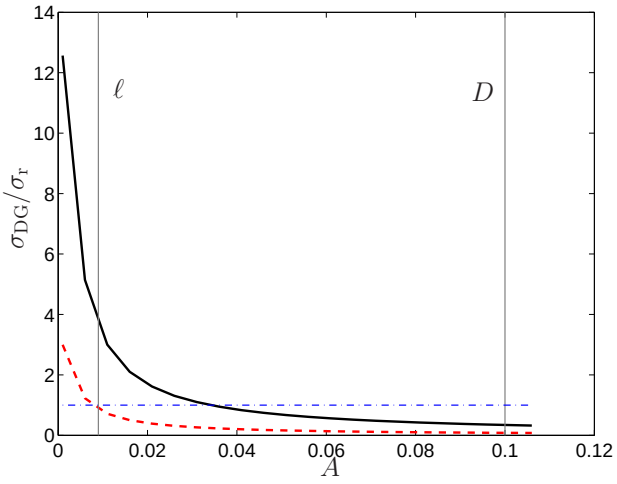

FIG. 8. (Color online) Plot of σ_{DG}/σ_r (ratio of Donnelly-Glaberson and vortex reconnection frequencies) vs wave amplitude A (cm), for thermally (dashed, red line) and mechanically (solid line) driven turbulence; the (blue) dot-dashed line represents $\sigma_{DG} = \sigma_r$.

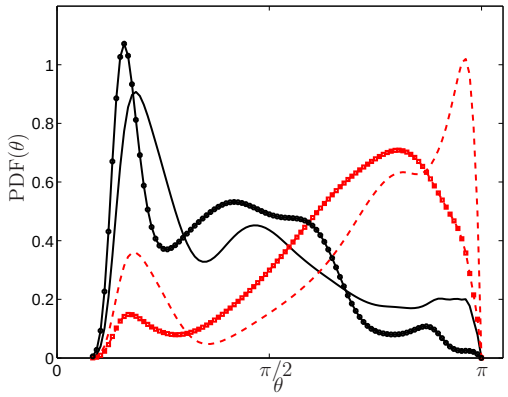

FIG. 9. (Color online) The probability density function (PDF) of the angle between reconnecting vortices, θ. Thermally-driven turbulence: at $T = 2.1\ K$ (dashed red line) and at $T = 1.9\ K$ (solid red squares); mechanically-driven turbulence: at $T = 2.1\ K$ (solid black line) and at $T = 1.9\ K$ (solid black line with solid black circles). Note that for thermally-driven turbulence the distribution peaks at large θ, whereas for mechanically-driven turbulence it peaks at small θ.

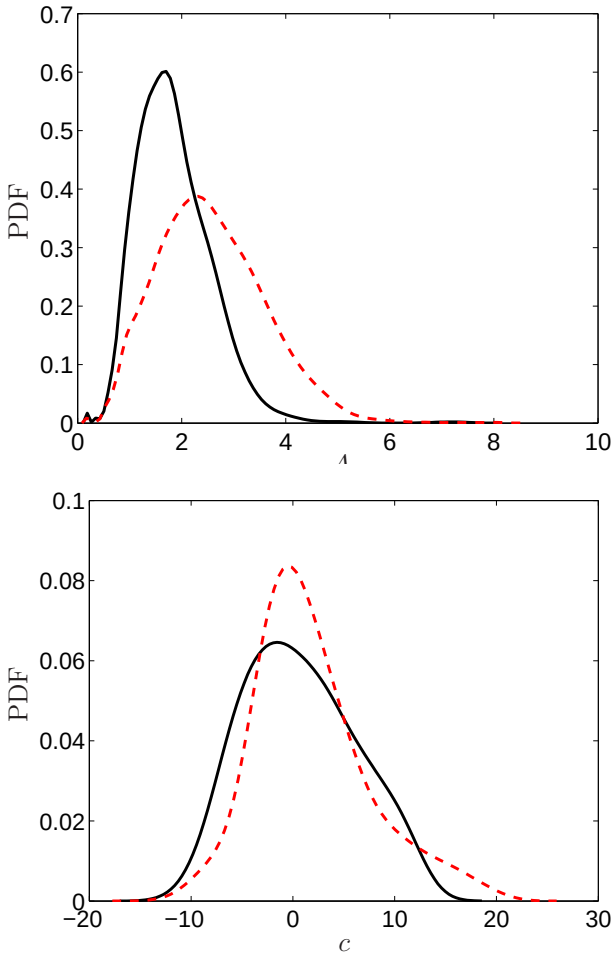

FIG. 10. (color online) Probability density functions (PDF) of the fitting parameters A (top) and c (s^{-1}) (bottom) of Eq. 7. Solid black line: mechanically-driven turbulence; dashed red line: thermally-driven turbulence.

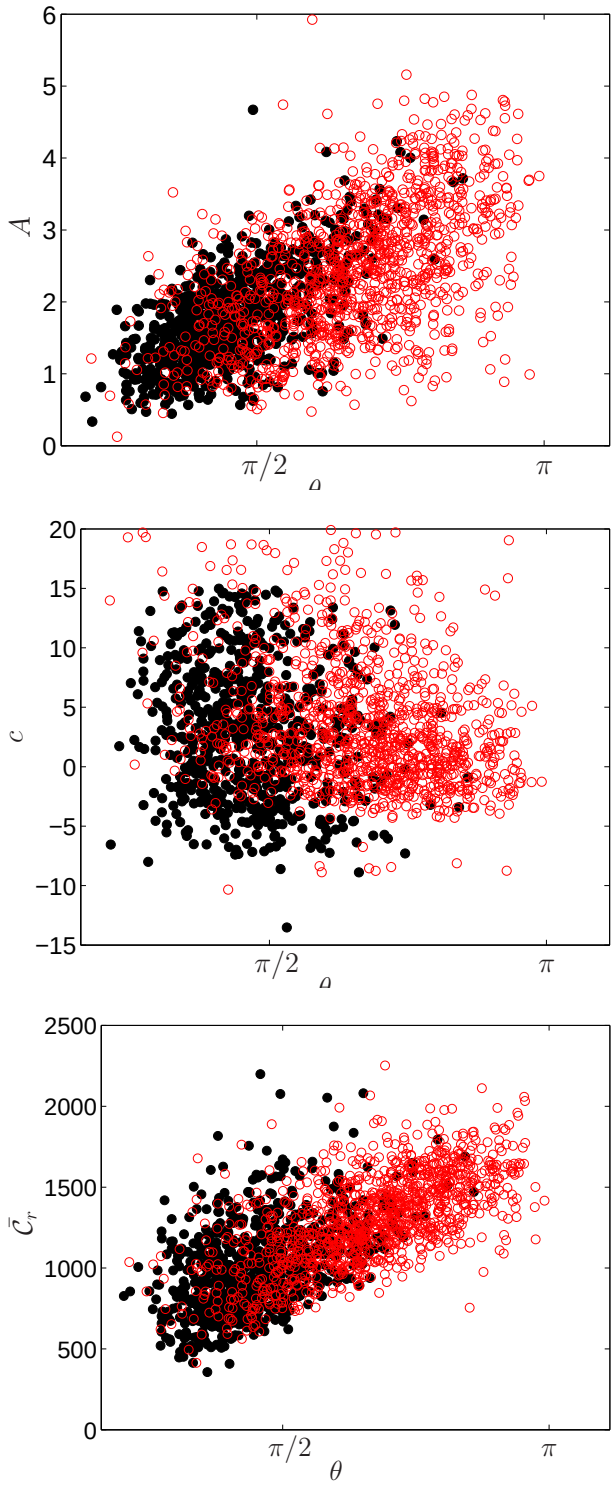

FIG. 11. (color online) Scatter plots of the fitting parameters A (top) and c (middle) of Eq. 7 vs the angle, θ, between the reconnecting vortices. The bottom figure shows the mean curvature $\bar{\mathcal{C}}_r$ of the reconnecting vortex segments vs the angle θ. Solid black points: mechanically-driven turbulence; open red circles: thermally-driven turbulence.